



ELSEVIER

Contents lists available at ScienceDirect

Comptes Rendus Chimie

www.sciencedirect.com



Full paper/Mémoire

Exploring the activities of vanadium, niobium, and tantalum PNP pincer complexes in the hydrogenation of phenyl-substituted $C\equiv N$, $C=N$, $C\equiv C$, $C=C$, and $C=O$ functional groups[☆]

Zhihong Wei, Kathrin Junge, Matthias Beller, Haijun Jiao^{*}

Leibniz-Institut für Katalyse e.V. an der Universität Rostock, Albert-Einstein-Straße 29a, 18059 Rostock, Germany

ARTICLE INFO

Article history:

Received 15 March 2017

Accepted 7 September 2017

Available online 16 October 2017

Keywords:

d5 Metal PNP complexes

Hydrogenation

Unsaturated functional groups

DFT

ABSTRACT

The structures and stability of the designed PNP pincer amido $M(NO)_2(PNP)$ and amino $^H M(NO)_2(PN^H P)$ complexes [$M = V, Nb, \text{ and } Ta, PNP = N(CH_2CH_2P(isopropyl)_2)_2, PN^H P = HN(CH_2CH_2P(isopropyl)_2)_2$] and their hydrogenation mechanisms for phenyl-substituted unsaturated functional groups have been explored at the B3PW91 level of density functional theory. Under H_2 environment, these conjugated complexes can form equilibrium and fulfill the criteria of metal–ligand cooperated bifunctional hydrogenation catalysts. For the hydrogenation of $Ph-C\equiv N$, $Ph-CH=NH$, $Ph-CH=NH-Ph$, $Ph-CH=N-CH_2Ph$, $Ph-C\equiv CH$, $Ph-CH=CH_2$, $Ph-CHO$, and $Ph-CO-CH_3$, the reaction prefers either a two-step or one-step mechanism for the hydridic $M-H$ and protonic $N-H$ transfer. These results clearly show that the $V, Nb, \text{ and } Ta$ complexes are promising catalysts for the hydrogenation reactions, and these provide experimental challenges.

© 2017 Académie des sciences. Published by Elsevier Masson SAS. All rights reserved.

1. Introduction

Catalytic hydrogenation of unsaturated compounds is indeed very important for organic synthesis as well as chemical and pharmaceutical industry [1,2], and homogeneous hydrogenation catalyzed by bifunctional metal–ligand–cooperated catalysts is one of the most promising pathways [3–25]. Pioneering studies of bifunctional catalysts were reported by Shvo and co-workers and Noyori and co-workers [4,5,26–30]. Noyori's theoretical study on the highly efficient bifunctional chiral Ru^{II} amido catalyst revealed that hydrogenation of unsaturated functional groups $C=X$ ($X=O, N$) takes place by metal–ligand

cooperation in an outer sphere manner via a six-membered transition state [3–5].

On the basis of metals and ligands, there are two types of bifunctional catalysts [31]. One undergoes the aromatization and dearomatization interconversion, such as the Shvo catalysts via $O-H$ bond and the Milstein catalysts via $C-H$ bond [26,27,32,33]. Another one involves the metal–ligand cooperation, such as the Noyori, Morris, and Beller catalysts via $N-H$ bond [3–5,34,35]. Among these catalysts, the pincer type complexes by Milstein and Beller have attracted much attention because such tridentate ligands can cover much of the coordination sphere and offer control over the vacant coordination sites with enhanced activity and stability [6].

Because the catalytic properties of a catalyst are generally determined by its electronic structure, design and screen of new catalysts are an integrated molecular approach [4,36]. The nature of noninnocent pincer ligands facilitating the hydride and proton transfer in the secondary sphere manner

[☆] Special memorial issue in honor of François Gault in the *Comptes rendus Chimie*, entitled “Advances in catalytic reactivity and specific mechanisms of nanostructured catalysts”.

^{*} Corresponding author.

E-mail address: Haijun.jiao@catalysis.de (H. Jiao).

allows for fine-tuning electronic structure of metal individually without significant change in the coordination geometry [23,24,37]. Several pincer-type complexes on the basis of metal substitution have been prepared and applied for the hydrogenation of nitriles, alkynes, alkenes, aldehydes, ketones, and esters as well as transfer hydrogenation [6–25]. Examples are the complexes of Mo and W [19,20,24], Mn [17,18], Fe [15,16], Ru [35,38], Os [21,22], Co [39,40], and Ir [23]. As metal screening and mechanism elucidation are limited by considerable amount of experimental work, electronic structure calculations are playing an important role in the design of new catalysts [23,36,37] and excellent pioneer work has been done [41–44]. There are also recent corresponding theoretical studies about the detailed mechanisms of hydrogenation and dehydrogenation as well as transfer hydrogenation [38,43,45–51].

In our previous work, we explored the hydrogenation of $\text{CH}_3\text{—C}\equiv\text{N}$, $\text{Ph—CO}_2\text{CH}_3$, and Ph—CHO by using the $d^8\text{—M}^{\text{II}}$ PNP pincer complexes ($\text{M} = \text{Fe, Ru, and Os}$). For the d^5 metals, to the best of our knowledge, only the $[\text{Nb}^{\text{IV}}\text{Cl}_3(\text{N}(\text{CH}_2\text{CH}_2\text{P}^i\text{Pr}_2)_2)]$ and $[\text{Nb}^{\text{III}}\text{Cl}_2(\text{N}(\text{CH}_2\text{CH}_2\text{P}^i\text{Pr}_2)_2)]$ complexes were prepared [52], but neither testing nor characterization of their catalytic activity was reported experimentally and theoretically. Herein, we explored the hydrogenation of phenyl-substituted $\text{C}\equiv\text{N}$, $\text{C}=\text{N}$, $\text{C}\equiv\text{C}$, $\text{C}=\text{C}$, and $\text{C}=\text{O}$ functional groups by $d^5\text{—M}^{\text{I}}$ PNP pincer complexes by means of density functional theory computation.

2. Computational details

2.1. Method

In our previous work, we found that B3PW91 gas phase calculations give results in excellent agreement with the experimentally observed stability and reactivity of the amido (M-PNP) and amino (H-M-PN^HP) complexes ($\text{M} = \text{Fe, Ru, Os, Ir, Mn, Mo, and W}$); the reaction energies as calculated from other methods, which include solvation effects, do not account for the possible equilibrium under the reaction conditions [23,38,45,53]. Because there are no experimental results available to validate the computational methods for these d^5 metal complexes, we used the gas phase B3PW91 method in our calculations by using the Gaussian 09 program [54]. All structures were optimized at the B3PW91 [55] level with the TZVP [56] basis set (LANL2DZ [57] for metals). All optimized structures were characterized either as energy minimums without imaginary frequencies or transition states with only one imaginary mode by frequency calculations, and the imaginary model connects the initial and the final states. The thermal correction to Gibbs free energy at 298 K from the frequency analysis was added to the total electronic energy. Natural atomic orbital and natural bond orbital analysis were carried out on the B3PW91 optimized structures with the natural bond orbital method [58,59]. The computed energetic data and Cartesian coordinates are listed in the Supplementary data.

2.2. Model

To establish the formal 18 valence electron complexes of the amido (M-PNP) complex (**1M**) and amino (H-M-PN^HP)

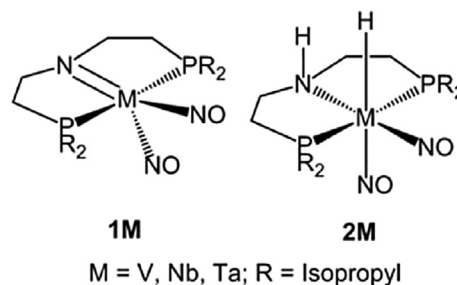
complex (**2M**), two NO ligands are coordinated to the metal center along with the PNP ligand (Scheme 1). Benchmark calculations show that the amido complex (**1M**) in C_1 symmetry due to different orientations of the isopropyl groups is more stable than the symmetrical isomer (C_s), and the amino (H-M-PN^HP) complex (**2M**) in C_s symmetry is more stable than the C_1 isomer (Table S1). Therefore, we used these more stable isomers for our energetic discussion and comparison (Scheme 1).

3. Results and discussion

3.1. Bonding of M-PNP (**1M**) and H-M-PN^HP (**2M**)

The B3PW91 computed bond distances of the distorted trigonal-bipyramid **1M** and distorted octahedral **2M** are given in Table S2. It shows that the M–N, M–P and M–NO bond lengths increase from V to Nb and then decrease to Ta, and this can be ascribed to the hybridization of metal and ligands [60]. Compared with the M–N distance in **1M**, the M–N distance in **2M** is elongated by 13.8, 11.9, and 12.3% for **2V**, **2Nb**, and **2Ta**, respectively, revealing extra bonding interaction in **1M**. In **2M**, the N–H bond length changes hardly, and the M–H bond length varies strongly, for example, the V–H bond (1.750 Å) is much shorter than the Nb–H (1.928 Å) and Ta–H (1.912 Å) bonds. In addition to these bond distances, we computed the N–O vibrational frequencies. On the basis of frequency calculations, the symmetrical and asymmetrical N–O stretching frequencies are 1605/1548, 1589/1515, and 1570/1500 cm^{-1} for **1V**, **1Nb**, and **1Ta**, respectively, as well as 1628/1532, 1594/1510, and 1576/1492 cm^{-1} for **2V**, **2Nb**, and **2Ta**, respectively.

In addition, natural localized molecular orbital analysis reveals an M=N double bond (one σ bond and one π bond) in **1Nb** and **1Ta**, and an M–N single bond in **2Nb** and **2Ta** (Table S3). The computed M–N Wiberg bond index in **1Nb** and **1Ta** is about double of that in **2Nb** and **2Ta** (Table S4), respectively. For the M–N_{PNP} σ bond in **1Nb** and **1Ta**, the N_{PNP} atom is sp hybridized and contributes more strongly to the M–N_{PNP} σ bond than the metal atom, and for the M–N_{PNP} π bond, the N_{PNP} atom has pure p character and has stronger contribution to the bond than the metal atom. The Nb atom in **1Nb** is slightly negatively charged, whereas the Ta atom in **1Ta** is slightly positively charged. In **2Nb** and **2Ta**, the metal atom is much more negatively charged, and the N_{PNP} atom is sp³ hybridized and contributes more strongly to the M–N_{PNP} σ bond than the metal atom. All



Scheme 1. Amido (**1M**) and amino (**2M**) complexes.

these show the polarization of the N=M and N–M bonds. In **1Nb** and **1Ta**, the M–NO bond also has double bond character (one σ bond and one π bond), and the metal atom contributes more strongly than that of the N atom of the NO ligand.

However, different binding properties in **1V** and **2V** are found. In **1V**, there is no σ bond between the V atom and the N atom of the PNP ligand, but there is a perpendicular π bond, mainly contributed by the N atom. Furthermore, there is a V \equiv N triple bond between the V atom and the N atom of the NO ligand, and the V metal atom contributes more strongly than the N atom to the σ bond and the two π bonds. In **2V**, there is also no σ bond between the V atom and the N atom of the PNP ligand, but a V \equiv N triple bond between the V atom and the N atom is found, and the V metal atom contributes more strongly than that of the N atom to the σ bond and the two π bonds. In **1V** and **2V**, the V atom is more negatively charged than the N atom of the PNP ligand.

Despite these bonding differences, it is noted that in **2M** the hydrogen atom (H_M) to metal is negatively charged, whereas the hydrogen atom (H_N) to the nitrogen atom is positively charged. This might fulfill the criteria of bifunctional hydrogenation catalysts. Therefore, we are interested in their stability and hydrogenation performances.

3.2. Catalysts interconversion ($1M + H_2 = 2M$)

At first, we calculated the catalyst interconversion between **1M** and **2M** by heterolytic H_2 addition [24,45]. The full potential energy surface is shown in the [Supplementary data \(Scheme S1\)](#). For the heterolytic H_2 addition, we located a concerted transition state in C_s symmetry. In the transition state of **2V**, **2Nb**, and **2Ta**, the forming M–H/N–H distances are 1.914/1.508, 2.103/1.494, and 2.072/1.496 Å, and the breaking H–H distances are 0.916, 0.934, and 0.937 Å, respectively. As shown on the simplified potential energy surface (Fig. 1), **1M** to **2M** interconversion has barrier of 102.5, 94.8, and 99.4 kJ/mol as well as is endergonic by 28.5, 30.4, and 28.7 kJ/mol for **2V**, **2Nb**, and **2Ta**

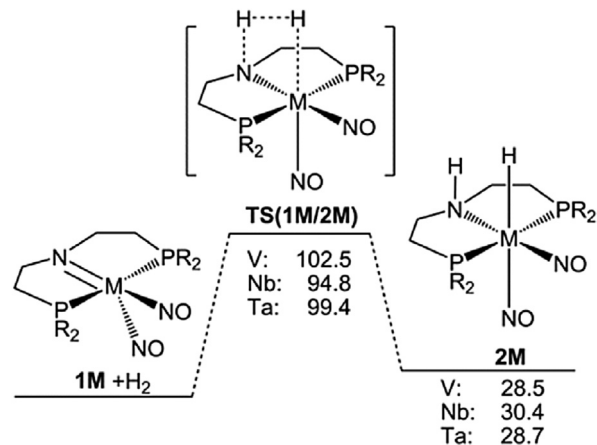


Fig. 1. Potential energy surface for M-PNP (**1M**) and H-M-PN^HP (**2M**) interconversion.

formation, respectively. The endergonic property indicates that the heterolytic H_2 addition is less favored kinetically and thermodynamically, in turn, the heterolytic H_2 elimination is more favored. Thus, **2M** can be only stable under high H_2 pressure and removal H_2 from the system should shift **2M** back to **1M**. This is very important for reactions with even higher barriers, because reactions with higher barriers can be kinetically hindered, although they are favorable thermodynamically (Fig. 1).

3.3. Hydrogenation of benzonitrile and imine

For Ph-C \equiv N hydrogenation to phenylmethanimine (Ph-CH=NH), a two-step asynchronous ionic mechanism [61] for the hydride (H_M) and proton (H_N) transfer was identified. The first transition state (TS- H_M) is the H_M transfer to the carbon atom of C \equiv N, resulting in the formation of the ionic intermediate (PhCHN⁻, **2M-int**). In TS- H_M , the breaking M–H distances are 1.822, 1.983, and 1.976 Å, and the forming C–H distances are 1.726, 1.741, and 1.664 Å, for **2V**, **2Nb**, and **2Ta**, respectively. The barriers of H_M transfer are 74.8, 66.1, and 68.9 kJ/mol for **2V**, **2Nb**, and **2Ta**, respectively, and the formation of **2M-int** is endergonic by 64.4, 55.2, and 63.7 kJ/mol for **2V**, **2Nb**, and **2Ta**, respectively. The second transition state (TS- H_N) is the H_N transfer from N_{PNP} to N_{PhCN} , and the breaking/forming N–H distances are 1.214/1.382, 1.211/1.392, and 1.203/1.400 Å for **2V**, **2Nb**, and **2Ta**, respectively. Relative to **2M** and Ph-C \equiv N, the barriers of H_N transfer are 59.5, 50.2, and 59.6 kJ/mol for **2V**, **2Nb**, and **2Ta**, respectively. On the simplified potential energy surface (Fig. 2), TS- H_N is more stable than **2M-int** by 4.9, 5.0, and 4.1 kJ/mol for **2V**, **2Nb**, and **2Ta**, respectively. The whole hydrogenation is exergonic by 45.3, 47.2, and 45.5 kJ/mol for **2V**, **2Nb**, and **2Ta**, respectively. Starting from the amido complex (**1M**), the apparent free energy barriers

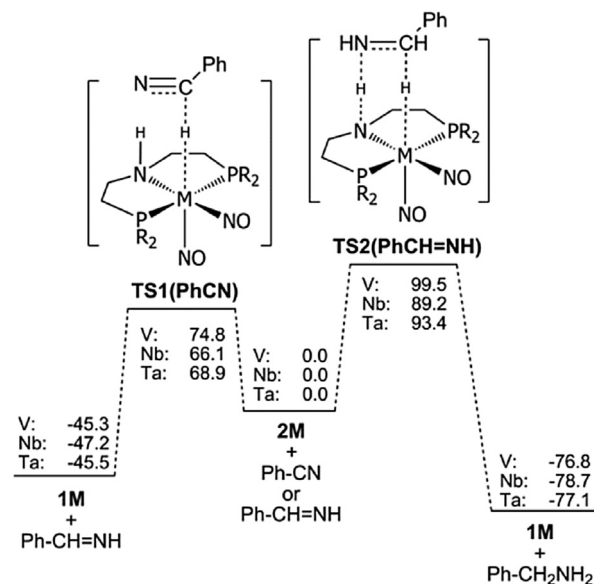


Fig. 2. Potential energy surface of benzonitrile and phenylmethanimine hydrogenation.

for the hydrogenation of Ph-C≡N are 103.3, 96.5, and 97.7 kJ/mol for **1V**, **1Nb**, and **1Ta**, respectively (Fig. 2).

For Ph-CH=NH hydrogenation to phenylmethanamine (Ph-CH₂-NH₂), a one-step mechanism is identified. This step has barrier of 99.5, 89.2, and 93.4 kJ/mol as well as is exergonic by 76.8, 78.7, and 77.1 kJ/mol for **2V**, **2Nb**, and **2Ta**, respectively. In the transition state for **2V**, **2Nb**, and **2Ta**, the breaking M–H/N–H distances are 1.865/1.056, 2.023/1.056, and 2.018/1.064 Å, respectively, and the forming C–H/N–H distances are 1.586/1.770, 1.604/1.776, and 1.545/1.735 Å, respectively. The transition state corresponds mainly to H_M transfer and followed by the subsequent H_N transfer without energy barrier. Compared to Ph-C≡N hydrogenation, Ph-CH=NH hydrogenation has higher barrier by 24.7, 23.1, and 24.5 kJ/mol for **2V**, **2Nb**, and **2Ta**, respectively, and Ph-CH=NH hydrogenation should be more difficult than Ph-C≡N hydrogenation. Starting from the amido complex (**1M**), the apparent free energy barriers for the hydrogenation of Ph-CH=NH are 128.0, 119.6, and 122.1 kJ/mol for **1V**, **1Nb**, and **1Ta**, respectively.

As a competitive reaction to Ph-CH=NH hydrogenation, depending on the reaction kinetics, the formed Ph-CH=NH and Ph-CH₂-NH₂ can condense to Ph-CH=N-CH₂-Ph by NH₃ release. Therefore, we computed the hydrogenation of Ph-CH=N-CH₂-Ph to Ph-CH₂-NH-CH₂-Ph and located one transition state for H_M transfer with the subsequent barrierless H_N transfer. In the transition state for **2V**, **2Nb**, and **2Ta**, the breaking M–H/N–H distances are 1.897/1.051, 2.023/1.045, and 2.019/1.051 Å, respectively, and the forming C–H/N–H distances are 1.551/1.835, 1.668/1.904, and 1.599/1.862 Å, respectively. As shown in Fig. 3, the reaction has barrier of 141.4, 125.3, and 130.8 kJ/mol as well as is exergonic by 63.3, 65.2, and 63.5 kJ/mol for **2V**, **2Nb**, and **2Ta**,

respectively. The energy barriers of Ph-CH=N-CH₂-Ph hydrogenation are 41.9, 36.2, and 37.5 kJ/mol higher than that of Ph-CH=NH for **2V**, **2Nb**, and **2Ta**, respectively. Starting from the amido complex (**1M**), the apparent free energy barriers for the hydrogenation of Ph-CH=N-CH₂-Ph are 170.0, 155.7, and 159.6 kJ/mol for **1V**, **1Nb**, and **1Ta**, respectively (Fig. 3).

For comparison, we computed *trans*-Ph-CH=N-Ph hydrogenation and found only one transition state corresponding mainly to H_M transfer. In the transition state for **2V**, **2Nb**, and **2Ta**, the breaking M–H/N–H distances are 1.860/1.036, 2.018/1.037, and 2.009/1.042 Å, respectively, and the forming C–H/N–H distances are 1.736/1.943, 1.780/1.947, and 1.723/1.903 Å, respectively. As shown in Fig. 3, *trans*-Ph-CH=N-Ph hydrogenation has barrier of 131.8, 114.8, and 120.4 kJ/mol for **2V**, **2Nb**, and **2Ta**, respectively, lower than that of Ph-CH=N-CH₂-Ph hydrogenation by 9.7, 10.5, and 10.4 kJ/mol for **2V**, **2Nb**, and **2Ta**, respectively. Starting from the amido complex (**1M**), the apparent free energy barrier for the hydrogenation of *trans*-Ph-CH=N-Ph is 160.3, 145.2, and 149.2 kJ/mol for **1V**, **1Nb**, and **1Ta**, respectively.

From Figs. 2 and 3, it is clearly seen that Ph-C≡N can be most easily hydrogenated to Ph-CH=NH, whereas hydrogenation of imines needs higher barrier and is more exergonic. For the hydrogenation of imines, Ph-CH=NH hydrogenation has the lowest barrier, followed by Ph-CH=N-Ph hydrogenation, whereas Ph-CH=N-CH₂-Ph hydrogenation has the highest barrier. In addition, the C≡N hydrogenation and the formation of **2M** have very close barriers (102.5 kJ/mol for **2V** formation vs 103.3 kJ/mol for C≡N hydrogenation, 94.8 kJ/mol for **2Nb** formation vs 96.5 kJ/mol for C≡N hydrogenation, and 99.4 kJ/mol for **2Ta** formation vs 97.7 kJ/mol for C≡N hydrogenation). For C=N hydrogenation, the second step of C=N hydrogenation is the rate-determining step for **2V**, **2Nb**, and **2Ta**. Starting from the amido complex (**1M**), the apparent barriers of the hydrogenation of Ph-C≡N, Ph-CH=NH, and Ph-CH=N-Ph are much higher than the barrier of H₂ elimination from **2M** to **1M**, high H₂ pressure is needed for the stability of **2M** and the effective hydrogenation.

3.4. Hydrogenation of phenylacetylene and styrene

Apart from hydrogenation of Ph-C≡N, we computed the sequential hydrogenation of phenylacetylene (Ph-C≡CH). The full potential energy surface is shown in the Supplementary data (Scheme S6) and the simplified one is used for discussion and comparison (Fig. 4). In contrast to Ph-C≡N, there are two C atoms in Ph-C≡CH and therefore two possibilities for H_M transfer. For the H_M transfer to C–H and the H_N transfer to Ph-C, we located one-step transition state, and the barrier is 84.6, 84.8, and 92.0 kJ/mol for **2V**, **2Nb**, and **2Ta**, respectively. Starting from the amido complex (**1M**), the apparent free energy barrier for the hydrogenation of Ph-C≡CH is 113.1, 115.2, and 120.8 kJ/mol for **1V**, **1Nb**, and **1Ta**. In the transition state for **2V**, **2Nb**, and **2Ta**, the breaking M–H/N–H distances are 1.825/1.024, 2.004/1.025, and 2.000/1.027 Å, respectively, and the forming C–H/N–H distances are 1.669/2.346, 1.661/2.359, and 1.602/2.302 Å, respectively. For H_M transfer to Ph-C and H_N transfer to C–H,

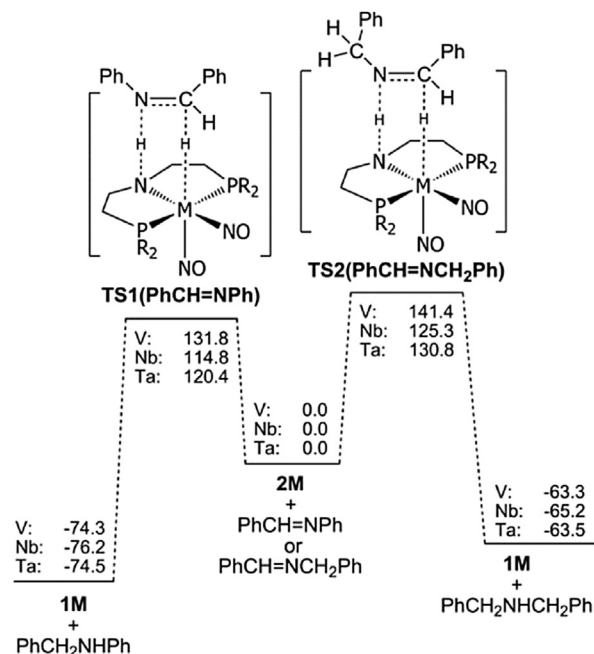


Fig. 3. Potential energy surface of PhCH=NCH₂Ph and PhCH=NPh hydrogenation.

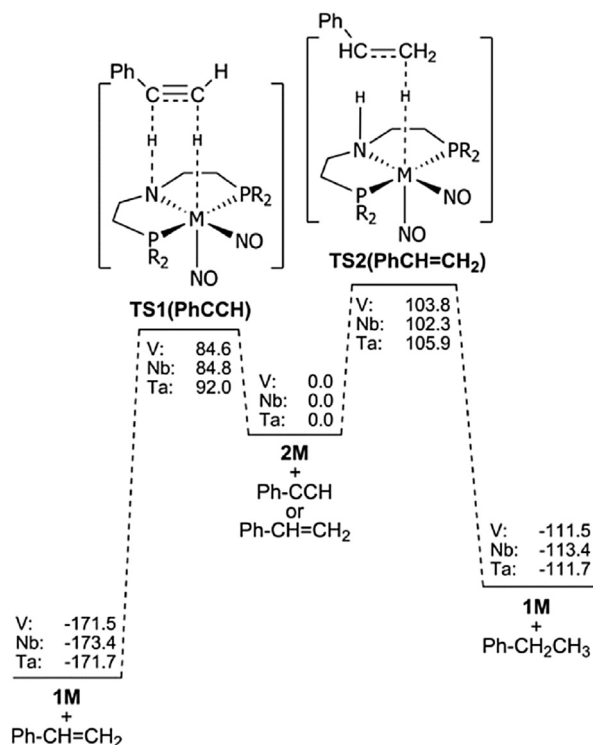


Fig. 4. Potential energy surface of phenylacetylene and styrene hydrogenation.

alternatively, we located a two-step asynchronous ionic mechanism with two transition states (Scheme S7). For the first transition state, the barriers of H_M transfer are 117.6, 111.1, and 114.0 kJ/mol for **2V**, **2Nb**, and **2Ta**, respectively. For the second transition state, the barriers of H_N transfer are 116.0, 111.6, and 120.9 kJ/mol for **2V**, **2Nb**, and **2Ta**, respectively. It clearly shows that H_M transfer to C–H and H_N transfer to Ph–C are more favored kinetically than H_M transfer to Ph–C and H_N transfer to C–H by 33.0, 26.3, and 22.0 kJ/mol for **2V**, **2Nb**, and **2Ta**, respectively. Starting from the amido complex (**1M**), the apparent free energy barriers for the hydrogenation of Ph–C≡CH are 103.1, 115.2, and 120.7 kJ/mol for **1V**, **1Nb**, and **1Ta**, respectively (Fig. 4).

As the counterpart of Ph–CH=NH, we computed styrene (Ph–CH=CH₂) hydrogenation into ethylbenzene (Ph–CH₂CH₃). In contrast to Ph–CH=NH hydrogenation, we found a two-step ionic mechanism. The simplified potential energy surface is shown in Fig. 4, and the full potential energy surface is shown in the Supplementary data (Scheme S8). The first step is the H_M transfer to the CH₂ carbon (β -carbon) and the second step is H_N transfer from N_{PNP} to the Ph–CH carbon (α -carbon). In the first transition state (TS- H_M), the breaking M–H distances are 1.855, 2.033, and 2.030 Å, and the forming C–H distances are 1.617, 1.613, and 1.556 Å, for **2V**, **2Nb**, and **2Ta**, respectively. In the second transition state (TS- H_N), the breaking/forming N–H distances are 1.196/1.558, 1.178/1.597, and 1.158/1.634 Å for **2V**, **2Nb**, and **2Ta**, respectively. As shown in Fig. 4, the barriers of H_M transfer to the CH₂ carbon are 103.8, 102.3, and 105.9 kJ/mol as well as the barriers of H_N transfer are

87.2, 80.6, and 95.2 kJ/mol for **2V**, **2Nb**, and **2Ta**, respectively. For Ph–CH=CH₂ hydrogenation, the reaction is exergonic by 111.5, 113.4, and 111.7 kJ/mol for **2V**, **2Nb**, and **2Ta**, respectively. Starting from the amido complex (**1M**), the apparent free energy barriers for the hydrogenation of Ph–CH=CH₂ are 132.3, 132.7, and 134.6 kJ/mol for **1V**, **1Nb**, and **1Ta**, respectively.

Fig. 4 shows clearly that Ph–C≡CH hydrogenation has lower barrier and is more exergonic than Ph–CH=CH₂ hydrogenation. In addition, C=C hydrogenation is the rate-determining step. On the basis of the whole potential energy surface, the hydrogenation of C≡C and C=C bonds is the rate-determining step for metals of **V**, **Nb**, and **Ta**. Because the apparent barriers of the hydrogenation of Ph–C≡CH, Ph–CH=CH₂ starting from the amido complex (**1M**) are much higher than the barrier of H₂ elimination from **2M** to **1M**, high H₂ pressure is needed to enhance the stability of **2M** for the hydrogenation reactions.

3.5. Hydrogenation of benzaldehyde and acetophenone

For benzaldehyde (Ph–CHO) hydrogenation, a two-step asynchronous ionic mechanism is identified (Fig. 5). The full potential energy surfaces are shown in the Supplementary data (Scheme S9). Initially, a transition state for H_M transfer to the carbon atom of CH=O corresponding to the M–H bond breaking and the C–H bond forming was located (TS- H_M). H_M transfer results in the formation of the ionic intermediate (Ph–CH₂O[−], **M-int**). Subsequently, a transition state for H_N transfer (TS- H_N) corresponding to N_{PNP} –H bond breaking and O_{PhCH_2O} –H bond forming is located. In the first transition state (TS- H_M), the breaking M–H distances are 1.825, 1.983, and 1.972 Å, and the forming C–H distances are 1.842, 1.902, and 1.819 Å for **2V**, **2Nb**, and **2Ta**, respectively. In the second transition state (TS- H_N), the breaking/forming N–H distances are 1.246/1.211, 1.182/1.328, and 1.085/1.542 Å for **2V**, **2Nb**, and **2Ta**, respectively. As shown in Fig. 5, the barriers of H_M

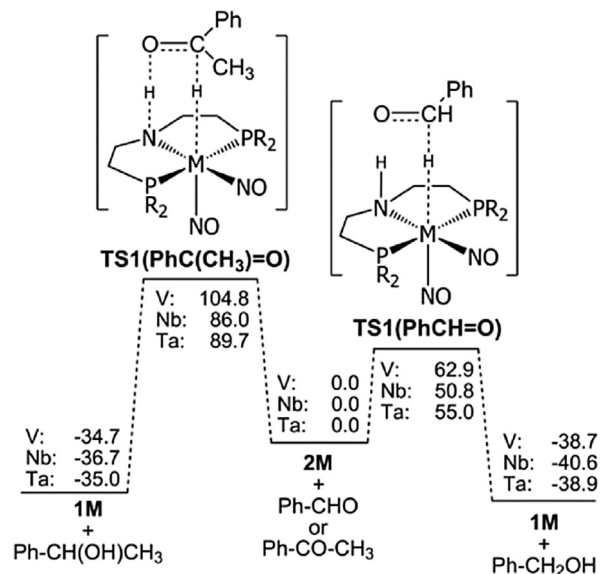


Fig. 5. Potential energy surface of benzaldehyde and acetophenone hydrogenation.

transfer are 62.9, 50.8, and 55.0 kJ/mol for **2V**, **2Nb**, and **2Ta**, respectively, and the formation of the **M-int** is endergonic by 28.5, 18.8, and 28.2 kJ/mol for **2V**, **2Nb**, and **2Ta**, respectively. In addition, the barriers of H_N transfer are 24.5, 14.7, and 43.7 kJ/mol, which is 38.3, 36.0, and 11.3 kJ/mol lower than that of H_M transfer for **2V**, **2Nb**, and **2Ta**, respectively. Starting from the amido complex (**1M**), the apparent free energy barriers for the hydrogenation of Ph-CHO are 91.4, 81.2, and 83.8 kJ/mol for **1V**, **1Nb**, and **1Ta**, respectively (Fig. 5).

For the hydrogenation of acetophenone (Ph-COCH₃), we found a one-step mechanism. In the transition state for **2V**, **2Nb**, and **2Ta**, the breaking M–H/N–H distances are 1.889/1.036, 2.031/1.035, and 2.016/1.038 Å, respectively, and the forming C–H/N–H distances are 1.770/1.780, 1.816/1.790, and 1.749/1.760 Å, respectively. The barrier is 104.8, 86.0, and 89.7 kJ/mol for **2V**, **2Nb**, and **2Ta**, respectively (Scheme S10), and the reaction is exergonic by 34.7, 36.7, and 35.0 kJ/mol for **2V**, **2Nb**, and **2Ta**, respectively. Most importantly, the barriers of benzaldehyde hydrogenation are lower than those of Ph-COCH₃ hydrogenation, and this indicates that Ph-CHO hydrogenation is more favored kinetically than Ph-COCH₃ hydrogenation. Furthermore, Ph-CHO hydrogenation is more favored thermodynamically than Ph-COCH₃ hydrogenation. Compared with the barrier of H₂ elimination from **2M** to **1M**, which is lower than that of acetophenone hydrogenation and higher than that of benzaldehyde hydrogenation, high H₂ pressure is needed to enhance the stability of **2M** for the hydrogenation. In addition, catalyst hydrogenation is the rate-determining step for Ph-CHO hydrogenation, whereas acetophenone hydrogenation is the rate-determining step. Starting from the amido complex (**1M**), the apparent free energy barriers for the hydrogenation of Ph-COCH₃ are 133.3, 116.4, and 118.5 kJ/mol for **1V**, **1Nb**, and **1Ta**. On the basis of the whole potential energy surface, **2M** formation is the rate-determining step for CH=O hydrogenation for **V**, **Nb**, and **Ta**, whereas C(CH₃)=O hydrogenation is the rate-determining step for **V**, **Nb** and **Ta**. Because the apparent barrier of the hydrogenation of Ph-CHO, Ph-COCH₃ starting from the amido complex (**1M**) is much higher than the barrier of H₂ elimination from **2M** to **1M**, high H₂ pressure can enhance the stability of **2M** for the hydrogenation reactions.

In addition, we compared the structures and stability of the Fe-amido and Fe-amino [Fe-PNP(CO)(H) and H–Fe–PN^HP(CO)(H)] complexes as well as their hydrogenation for Ph-C≡N, Ph-C≡CH, and Ph-CH=O with those of the d⁵ metal complexes (Table 1). For the stepwise reactions, we used the effective barriers. Starting from the amido complex (**1M**), the formation of the amino complex (**2M**) of the d⁵ metals (M = V, Nb, and Ta) needs higher

barrier (102.5, 94.8, and 99.4 kJ/mol, respectively) and is stronger endergonic (28.5, 30.4, and 28.7 kJ/mol, respectively) than that of the corresponding Fe complexes (82.8 vs 2.4 kJ/mol). These reveal that the **2M** complexes of the d⁵ metals are less stable than the corresponding Fe complex, and even higher H₂ pressure is needed to maintain the stability of the d⁵ amino complexes. On the basis of the barrier of **2M** dehydrogenation, the corresponding amino Fe complex should be more stable than **2V**, **2Nb**, and **2Ta** under the same hydrogen atmosphere (Table 1).

For the hydrogenation of Ph-C≡N, Ph-C≡CH, and Ph-CH=O starting from the amino complexes (**2M**) of the d⁵ metals, the effective barriers of the hydrogenation of Ph-C≡N and Ph-CH=O are higher than that of Ph-C≡CH hydrogenation by about 10 kJ/mol for **2V** as well as by about 20 kJ/mol for **2Nb** and **2Ta**, indicating that Ph-C≡N and Ph-CH=O can be more easily hydrogenated than Ph-C≡CH. The same trend is found for the corresponding Fe complex, although the effective barrier differences are 5 kJ/mol.

For the hydrogenation of Ph-C≡N and Ph-CH=O, the effective barrier has the decreasing order of V > Ta > Nb > Fe. For the hydrogenation of Ph-C≡CH, the effective barrier has the decreasing order of Ta > Nb > V > Fe. This clearly shows that the Fe complexes are the most effective catalysts for the hydrogenation of Ph-C≡N, Ph-C≡CH, and Ph-CH=O.

4. Conclusion

In this work, we computed the structures and stability of the amido (M-PNP) (**1M**) and amino (H-M-PN^HP) (**2M**) complexes (M = V, Nb, and Ta) as well as their hydrogenation mechanisms for the phenyl-substituted C≡N, C=N, C≡C, C=C, and C=O functional groups at the B3PW91 level of density functional theory.

On the basis of the computational results, we can make some predicative judgment about the hydrogenation of these V, Nb, and Ta PNP complexes. At first, the interconversion from **1M** to **2M** complex is via heterolytic addition of H₂. The endergonic property reveals that **2M** complexes can only be stable under H₂ environment.

For all these hydrogenation reactions by using these d⁵ PNP complexes, we found the same reaction mechanisms, that is, the hydrogenation of Ph-C≡N, Ph-CH=CH₂, and Ph-CHO undergoes a two-step mechanism, where the first step is the M–H transfer, followed by an ionic intermediate, and the second step is the N–H transfer, whereas that of Ph-C≡CH, Ph-CH=NH, Ph-CH=NH-Ph, Ph-CH=N–CH₂Ph, and Ph-CO–CH₃ prefers a one-step mechanism, and only transition state of M–H transfer could be located. The

Table 1

Gibbs free energy barriers (ΔG^\ddagger , kJ/mol) and effective barriers ($\Delta G^\ddagger_{\text{eff}}$, kJ/mol) for **2M** formation as well as Ph-C≡N, Ph-C≡CH, and Ph-CH=O hydrogenation.

Metals	1M + H ₂ = 2M	Ph-C≡N + H ₂ = Ph-CH=NH		Ph-C≡CH + H ₂ = Ph-CH=CH ₂		Ph-CH=O + H ₂ = Ph-CH ₂ -OH	
	ΔG^\ddagger	ΔG^\ddagger	$\Delta G^\ddagger_{\text{eff}}$	ΔG^\ddagger	$\Delta G^\ddagger_{\text{eff}}$	ΔG^\ddagger	$\Delta G^\ddagger_{\text{eff}}$
V	102.5 [74.0] ^a	74.8	103.3	84.6	113.1	62.9	102.5
Nb	94.8 [64.4] ^a	66.1	96.5	84.8	115.2	50.8	94.8
Ta	99.4 [70.7] ^a	68.9	99.4	92.0	120.8	55.2	99.4
Fe	82.8 [80.4] ^a	77.0	82.8	85.4	87.8	56.7	82.8

^a The barrier of the reverse reaction is given in square bracket.

barrier has the increasing order of $\text{Ph-C}\equiv\text{N} < \text{Ph-CH}=\text{NH} < \text{Ph-CH}=\text{N-Ph} < \text{Ph-CH}=\text{N-CH}_2\text{-Ph}$. The hydrogenation of $\text{C}\equiv\text{C}$ and $\text{C}\equiv\text{N}$ bonds has lower barrier than that of $\text{C}=\text{C}$ and $\text{C}=\text{N}$ bonds, respectively. In addition, the barrier of $\text{C}\equiv\text{C}$ and $\text{C}=\text{C}$ bonds is lower than that of $\text{C}\equiv\text{N}$ and $\text{C}=\text{N}$ bonds. Furthermore, Ph-COCH_3 hydrogenation has higher barrier than Ph-CHO hydrogenation. Under high H_2 pressure, all these d^5 complexes which exhibit similar intrinsic energy barrier and higher effective energy barrier can be as effective catalysts for the hydrogenation reactions as the well-known corresponding Fe complexes. All of these provide the basis for experimental proofs.

Acknowledgments

This work was supported by the state of Mecklenburg-Vorpommern and the Leibniz Association (Leibniz Competition, SAW-2016-LIKAT-1).

Appendix A. Supplementary data

Supplementary data related to this article can be found at <https://doi.org/10.1016/j.crci.2017.09.001>.

References

- [1] P.G. Andersson, I.J. Munslow, *Modern Reduction Methods*, Wiley-VCH, Weinheim, Germany, 2008.
- [2] J.G. De Vries, L. Lefort, *The Handbook of Homogeneous Hydrogenation*, Wiley-VCH, Weinheim, Germany, 2008.
- [3] M. Yamakawa, H. Ito, R. Noyori, *J. Am. Chem. Soc.* 122 (2000) 1466–1478.
- [4] R. Noyori, M. Yamakawa, S. Hashiguchi, *J. Org. Chem.* 66 (2001) 7931–7944.
- [5] R. Noyori, S. Hashiguchi, *Acc. Chem. Res.* 30 (1997) 97–102.
- [6] C. Gunanathan, D. Milstein, *Chem. Rev.* 114 (2014) 12024–12087.
- [7] G. Chelucci, S. Baldino, W. Baratta, *Acc. Chem. Res.* 48 (2015) 363–379.
- [8] W. Kuriyama, T. Matsumoto, O. Ogata, Y. Ino, K. Aoki, S. Tanaka, K. Ishida, T. Kobayashi, N. Sayo, T. Saito, *Org. Process Res. Dev.* 16 (2012) 166–171.
- [9] J. Zhang, M. Gandelman, D. Herrman, G. Leitus, L.J.W. Shimon, Y. Ben-David, D. Milstein, *Inorg. Chim. Acta* 359 (2006) 1955–1960.
- [10] W. Zuo, A.J. Lough, Y.F. Li, R.H. Morris, *Science* 342 (2013) 1080–1083.
- [11] T. Zell, B. Butschke, Y. Ben-David, D. Milstein, *Chem. Eur. J.* 19 (2013) 8068–8072.
- [12] T. Zell, Y. Ben-David, D. Milstein, *Catal. Sci. Technol.* 5 (2015) 822–826.
- [13] T. Zell, D. Milstein, *Acc. Chem. Res.* 48 (2015) 1979–1994.
- [14] E. Alberico, P. Sponholz, C. Cordes, M. Nielsen, H.-J. Drexler, W. Baumann, H. Junge, M. Beller, *Angew. Chem., Int. Ed.* 52 (2013) 14162–14166.
- [15] C. Bornschein, S. Werkmeister, B. Wendt, H. Jiao, E. Alberico, W. Baumann, H. Junge, K. Junge, M. Beller, *Nat. Commun.* 5 (2014) 4111.
- [16] S. Werkmeister, K. Junge, B. Wendt, E. Alberico, H. Jiao, W. Baumann, H. Junge, F. Gallou, M. Beller, *Angew. Chem., Int. Ed.* 53 (2014) 8722–8726.
- [17] S. Elangovan, M. Garbe, H. Jiao, A. Spannenberg, K. Junge, M. Beller, *Angew. Chem., Int. Ed.* 55 (2016) 15364–15368.
- [18] S. Elangovan, C. Topf, S. Fischer, H. Jiao, A. Spannenberg, W. Baumann, R. Ludwig, K. Junge, M. Beller, *J. Am. Chem. Soc.* 138 (2016) 8809–8814.
- [19] S. Chakraborty, O. Blacque, H. Berke, *Dalton Trans.* 44 (2015) 6560–6570.
- [20] S. Chakraborty, H. Berke, *ACS Catal.* 4 (2014) 2191–2194.
- [21] M. Bertoli, A. Choualeb, A.J. Lough, B. Moore, D. Spasyuk, D.G. Gusev, *Organometallics* 30 (2011) 3479–3482.
- [22] A. Acosta-Ramirez, M. Bertoli, D.G. Gusev, M. Schlaf, *Green Chem.* 14 (2012) 1178–1188.
- [23] K. Junge, B. Wendt, H. Jiao, M. Beller, *ChemCatChem* 6 (2014) 2810–2814.
- [24] S. Chakraborty, O. Blacque, T. Fox, H. Berke, *Chem. Asian J.* 9 (2014) 328–337.
- [25] M. Perez, S. Elangovan, A. Spannenberg, K. Junge, M. Beller, *ChemSusChem* 10 (2017) 83–86.
- [26] Y. Blum, D. Czarkie, Y. Rahamim, Y. Shvo, *Organometallics* 4 (1985) 1459–1461.
- [27] Y. Shvo, D. Czarkie, Y. Rahamim, D.F. Chodosh, *J. Am. Chem. Soc.* 108 (1986) 7400–7402.
- [28] S. Hashiguchi, A. Fujii, J. Takehara, T. Ikariya, R. Noyori, *J. Am. Chem. Soc.* 117 (1995) 7562–7563.
- [29] J. Takehara, S. Hashiguchi, A. Fujii, S.-I. Inoue, T. Ikariya, R. Noyori, *Chem. Commun.* (1996) 233–234.
- [30] S.E. Clapham, A. Hadzovic, R.H. Morris, *Coord. Chem. Rev.* 248 (2004) 2201–2237.
- [31] C. Hou, Z. Zhang, C. Zhao, Z. Ke, *Inorg. Chem.* 55 (2016) 6539–6551.
- [32] J. Zhang, G. Leitus, Y. Ben-David, D. Milstein, *Angew. Chem., Int. Ed.* 45 (2006) 1113–1115.
- [33] L.A. Saudan, C.M. Saudan, C. Debieux, P. Wyss, *Angew. Chem., Int. Ed. Engl.* 119 (2007) 7617–7620.
- [34] T. Li, I. Bergner, F.N. Haque, M. Zimmer-De Juiis, D. Song, R.H. Morris, *Organometallics* 26 (2007) 5940–5949.
- [35] M. Nielsen, E. Alberico, W. Baumann, H.-J. Drexler, H. Junge, S. Gladiali, M. Beller, *Nature* 495 (2013) 85–89.
- [36] J.K. Nørskov, T. Bligaard, J. Rossmeisl, C.H. Christensen, *Nat. Chem.* 1 (2009) 37–46.
- [37] J. Choi, A.H.R. MacArthur, M. Brookhart, A.S. Goldman, *Chem. Rev.* 111 (2011) 1761–1779.
- [38] E. Alberico, A.J.J. Lennox, L.K. Vogt, H. Jiao, W. Baumann, H.-J. Drexler, M. Nielsen, A. Spannenberg, M.P. Checinski, H. Junge, M. Beller, *J. Am. Chem. Soc.* 138 (2016) 14890–14904.
- [39] R. Xu, S. Chakraborty, H. Yuan, W.D. Jones, *ACS Catal.* 5 (2015) 6350–6354.
- [40] S. Fu, N.-Y. Chen, X. Liu, Z. Shao, S.-P. Luo, Q. Liu, *J. Am. Chem. Soc.* 138 (2016) 8588–8594.
- [41] A.A. Latimer, A.R. Kulkarni, H. Aljama, J.H. Montoya, J.S. Yoo, C. Tsai, F. Abild-Pedersen, F. Stedt, J.K. Nørskov, *Nat. Mater.* 16 (2017) 225–229.
- [42] J.E. Sutton, W. Guo, M.A. Katsoulakis, D.G. Vlachos, *Nat. Chem.* 8 (2016) 331–337.
- [43] X. Yang, *ACS Catal.* 1 (2011) 849–854.
- [44] B. Mondal, F. Neese, S. Ye, *Inorg. Chem.* 55 (2016) 5438–5444.
- [45] H. Jiao, K. Junge, E. Alberico, M. Beller, *J. Comput. Chem.* 37 (2016) 168–176.
- [46] S. Qu, H. Dai, Y. Dang, C. Song, Z.-X. Wang, H. Guan, *ACS Catal.* 4 (2014) 4377–4388.
- [47] R. Xu, S. Chakraborty, S.M. Bellows, H. Yuan, T.R. Cundari, W.D. Jones, *ACS Catal.* 6 (2016) 2127–2135.
- [48] X. Yang, *ACS Catal.* 3 (2013) 2684–2688.
- [49] X. Yang, *Inorg. Chem.* 50 (2011) 12836–12843.
- [50] X. Yang, *ACS Catal.* 4 (2014) 1129–1133.
- [51] C. Hou, J. Jiang, Y. Li, Z. Zhang, C. Zhao, Z. Ke, *Dalton Trans.* 44 (2015) 16573–16585.
- [52] A.-R.H. Al-Soudani, P.G. Edwards, M.B. Hursthouse, K.M.A. Malik, *J. Chem. Soc. Dalton Trans.* (1995) 355–361.
- [53] Z. Wei, K. Junge, M. Beller, H. Jiao, *Catal. Sci. Technol.* 7 (2017) 2298–2307.
- [54] M.J. Frisch, G.W. Trucks, H.B. Schlegel, G.E. Scuseria, M.A. Robb, J.R. Cheeseman, G. Scalmani, V. Barone, G.A. Petersson, H. Nakatsuji, X. Li, M. Caricato, A. Marenich, J. Bloino, B.G. Janesko, R. Gomperts, B. Mennucci, H.P. Hratchian, J.V. Ortiz, A.F. Izmaylov, J.L. Sonnenberg, D. Williams-Young, F.L.F. Ding, J.G.F. Egidi, A.P.B. Peng, T. Henderson, D. Ranasinghe, V.G. Zakrzewski, N.R.J. Gao, W.L.G. Zheng, M.E.M. Hada, K. Toyota, R. Fukuda, J. Hasegawa, M. Ishida, T. Nakajima, Y. Honda, O. Kitao, H. Nakai, T. Vreven, K. Throssell, J. A.M. Jr., J.E. Peralta, F. Ogliaro, M. Bearpark, J.J. Heyd, E. Brothers, K.N. Kudin, V.N. Staroverov, T. Keith, R. Kobayashi, J. Normand, K. Raghavachari, A. Rendell, J.C. Burant, S.S. Iyengar, J. Tomasi, M. Cossi, J.M. Millam, M. Klene, C. Adamo, R. Cammi, J.W. Ochterski, R.L. Martin, K. Morokuma, O. Farkas, J.B. Foresman, D.J. Fox, *Gaussian Software, Version 09 Revision D01*, Gaussian Inc., Wallingford, CT, USA, 2009.
- [55] J.P. Perdew, *Phys. Rev. B* 33 (1986) 8822–8824.
- [56] A. Schäfer, C. Huber, R. Ahlrichs, *J. Chem. Phys.* 100 (1994) 5829–5835.
- [57] P.J. Hay, W.R. Wadt, *J. Chem. Phys.* 82 (1985) 299–310.
- [58] A.E. Reed, L.A. Curtiss, F. Weinhold, *Chem. Rev.* 88 (1988) 899–926.
- [59] F. Weinhold, *Discovering Chemistry with Natural Bond Orbitals*, John Wiley & Sons, Inc., Hoboken, New Jersey, 2012.
- [60] E.D. Jemmis, S. Roy, V.V. Burlakov, H. Jiao, M. Klahn, S. Hansen, U. Rosenthal, *Organometallics* 29 (2010) 76–81.
- [61] P.A. Dub, J.C. Gordon, *ACS Catal.* 7 (2017) 6635–6655.